Variable Mode Bidirectional LLC Resonant Converter With Dual Resonant Branches

Qinglin Zhao, Zhouzhou Wu, Shixiang Gao, Jing Yuan, Deyu Wang, *Member, IEEE*, and Hao Ding, *Member, IEEE*

***Abstract*—This article proposes a variable-mode bidirectional LLC resonant converter equipped with two resonant branches, which enables wide-range output voltage regulation within a limited switching frequency range. By regulating the driving signals of the switches, the converter can switch between two operating modes during forward operation: dual half-bridge mode and full-bridge plus half-bridge mode. Correspondingly, during reverse operation, it operates in dual-path voltage-doubling mode and single-path voltage-doubling mode. Frequency modulation is adopted in all operating modes, and synchronous rectification technology is also integrated. Throughout all operational phases, zero voltage switching is implemented for every active switching device, effectively minimizing switching losses and optimizing the overall energy conversion efficiency of the system. A 2.5 kW experimental platform has been built: in forward operation, the dc bus voltage on the primary side is maintained at 400 V, while the battery voltage on the secondary side can be adjusted within the range of 250–450 V, thereby achieving wide output voltage regulation; in reverse operation, the battery terminal voltage ranges from 250 to 450 V, enabling wide input voltage regulation.**

***Index Terms*—Bidirectional resonant converter, LLC, variable frequency, zero voltage switching (ZVS).**

I. Introduction

DRIVEN by the urgent demand to reduce fossil fuel consumption and protect the environment, research focus on new energy technologies has been increasingly intensive, which in turn has fueled the rapid development of the new energy vehicle (EV) industry in recent years [1], [2]. Bidirectional dc–dc converters enable bidirectional power transmission and offer advantages of smaller volume and lower cost compared to two separate unidirectional converters. Among them, isolated bidirectional dc–dc converters are widely applied in vehicle-to-grid (V2G) systems, energy storage systems, and power electronic transformers, thanks to their excellent reliability and stability [3], [4], [5]. Currently, a key research direction lies in exploring how to enable bidirectional converters to achieve wide-range voltage output in both forward and reverse directions while ensuring soft switching for power semiconductor devices[6].

LLC resonant converters are widely used for their simple topology, easy soft switching implementation, and high power density [7], [8], [9], [10], [11] adopt a hybrid LLC structure to improve efficiency, with output voltage regulated via phase shift modulation (PSM). Nevertheless, such hybrid structures inherently introduce multiple control loops and additional components, leading to higher costs and potential reliability risks. Moreover, achieving zero voltage switching (ZVS) in the LLC converter's lagging leg via PSM is challenging—an excessively large phase shift angle may even trigger diode reverse recovery issues.

Partial power LLC resonant converters are proposed in [12] and [13], which achieve voltage regulation via a partial power buck cell. Though classified as single-stage topologies, they require a similar number of switching devices as two-stage solutions. To reduce the number of switches, several true single-stage PWM-controlled LLC resonant topologies are developed in [14], [15], and [16]; their output voltage is regulated by adjusting the duty cycle of MOSFETs integrated into the voltage multiplier rectifier circuit. However, these topologies inevitably suffer from significant turn-OFF losses and asymmetrical resonant currents, increasing system design complexity.

Furthermore, the authors in [17], [18], and [19] proposed a multiresonant converter suitable for wide voltage ranges. By introducing a parallel resonant circuit with notch filtering, it uses the third harmonic for active power transmission, reducing reactive power circulation losses and improving efficiency. Yet, multiresonant converters have a limited input–output voltage conversion ratio, restricting their application in high-voltage scenarios. Additionally, multiple magnetic elements increase their manufacturing cost and complexity.

Zuo et al. [20] proposed a converter where the primary side realizes half-voltage/full-voltage inversion and the secondary side implements quadruple-voltage/double-voltage rectification. Coordinating switching states on both sides establishes three circuit modes, enabling a wide voltage gain range without additional switches or resonant components. Nevertheless, this topology is mainly suitable for low-current, high-voltage scenarios, and not applicable to high-power applications.

Received 1 September 2025; revised 13 November 2025; accepted 6 December 2025. Date of publication 11 December 2025; date of current version 25 February 2026. This work was supported in part by the Natural Science Foundation of Hebei under Grant E2023203148 and in part by the S&T Program of Qinhuangdao under Grant 202501A004. Recommended for publication by Associate Editor H. Wu. *(Corresponding author: Qinglin Zhao.)*

Qinglin Zhao, Zhouzhou Wu, Jing Yuan, Deyu Wang, and Hao Ding are with the School of Electrical Engineering and the Key Laboratory of Power Electronics for Energy Conservation and Drive Control of Hebei Province, Yanshan University, Qinhuangdao 066004, China (e-mail: powerzql@ysu.edu.cn; wuzhouzhou@stumail.ysu.edu.cn; yuanjing@ysu.edu.cn; wdy@ysu.edu.cn; dinghao@ysu.edu.cn).

Shixiang Gao is with Lite on Group, Nanjing 210000, China (e-mail: shane.gao@liteon.com).

Color versions of one or more figures in this article are available at https://doi.org/10.1109/TPEL.2025.3642970.

Digital Object Identifier 10.1109/TPEL.2025.3642970

Reconfiguring LLC resonant converter structures is also a popular research direction. The authors in [21], [22], and [23] proposed an improved high-efficiency LLC converter with two resonant tanks, realized by adding an extra resonant circuit. Controlling the drive signals of power switches allows these tanks to operate in different modes, achieving a wide voltage gain range, but the converter cannot support bidirectional power transfer. Fan et al. [24] puts forward a series transformer partial power regulation circuit, which uses series-connected low-voltage devices instead of high-voltage ones to reduce conduction losses. It realizes wide voltage regulation through cascaded buck circuits, yet the multibridge arm driving requires high-precision phase synchronization, increasing the complexity of the control circuit.

Xu et al. [25] discussed a new CLLC bidirectional resonant converter with a secondary-side capacitor, which can operate in step-down and step-up modes. However, its bidirectional operation has asymmetric characteristics due to different resonant networks, making parameter design more complex. The authors in [26] and [27] explored symmetric CLLC configurations, which improve operational symmetry to a certain extent but only achieve a slight gain reduction below unity, limiting their application in wide-voltage scenarios. The authors in [28] and [29] obtained good gain characteristics by adding optimized converters, auxiliary transformers, and magnetic gain components on both sides, but this increases the complexity of the resonant cavity circuit, posing significant challenges to analysis and design. Based on the concept of the multiresonator network, a type of LCLT resonant converter can be derived [30]. This converter operates at a variable frequency and enables ZVS in all switching operations.

Based on the converter proposed in [24], this article improves it and proposes a bidirectional LLC resonant converter based on dual-branch LLC (DBLLC). In this converter, active switches are configured on both the primary and secondary sides. Through precise control of the drive signals of these active switches and a dc-blocking capacitor was additionally installed on the secondary side, the converter can flexibly switch between multiple operating modes, enabling bidirectional power flow to adapt to different application scenarios. On the other hand, it expands the power level and achieves a wide voltage regulation range of 250–450 V, meeting the requirements of high-voltage fast charging. All active switches achieve soft switching across the entire load range, which effectively reduces switching losses, improves efficiency, and enhances the reliability and stability of the system. Overall, it is more in line with the practical engineering needs of high power, wide voltage, and bidirectional power transmission in scenarios such as new EVs and energy storage systems.

II. Working Principle of the Proposed Converter

The main circuit of the proposed variable-mode bidirectional LLC resonant converter is illustrated in Fig. 1. The primary side is connected to the dc bus U_1, while the secondary side is linked to the battery U_2. Specifically, the primary side is equipped with switches S_1–S_4, and the secondary side with switches S_5–S_8. This converter adopts a dual-resonant-branch

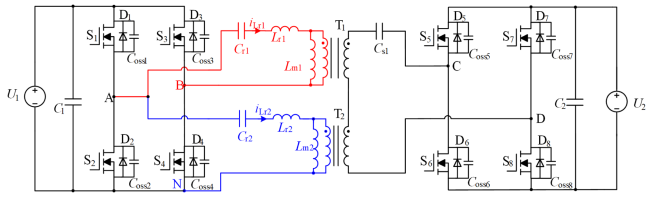

Fig. 1. Topology of the DBLLC converter

topology: two transformers form independent resonant circuits, with their primary windings connected in parallel and secondary windings connected in series. Sharing the same switching bridge arm, the two branches feature symmetric parameters, namely $L_{r1} = L_{r2} = L_r$, $L_{m1} = L_{m2} = L_m$, $C_{r1} = C_{r2} = C_r$, and turns ratio $n_1 = n_2 = n$.

By adjusting the driving signals of the active switches, the converter can flexibly switch between different operating modes. During forward operation, the primary side operates in either dual half-bridge (DHB) mode or full-bridge plus half-bridge (FHB) mode, while the secondary-side switches S_5–S_8 adopt synchronous rectification technology. In reverse operation, under the control of driving signals, switches S_5–S_8 form a full-bridge inverter, with the blocking capacitor C_{s1} used to suppress the bias magnetization of the transformers. Meanwhile, the primary-side switches S_1–S_4 operate in either dual-path voltage-doubling (DV) mode or single-path voltage-doubling (SV) mode. All operating modes employ frequency modulation for voltage regulation and integrate synchronous rectification technology, thereby ensuring efficient and stable operation of the converter under varying working conditions.

A. Dual Half-Bridge Mode

In DHB mode, shared bridge arm switches S_1 and S_2 operate complementarily with 50% duty cycle; S_3 is permanently OFF, and S_4 remains ON. The two transformers have parallel primary windings and series secondary windings. Coupling capacitor C_{s1} acts as a dc blocker without participating in resonance, making the circuit equivalent to a DHB LLC resonant converter as shown in Fig. 2(a).

The circuit input consists of square-wave voltages u_{AB} and u_{AN} with amplitude U_1. The amplitude of secondary voltage u_{CD} directly affects output voltage U_2 stability. Power distributes equally between the two transformers, and primary current i_{Lr} is the sum of the two transformer currents: $i_{Lr} = i_{Lr1} + i_{Lr2}$. Key operating waveforms in DHB mode are shown in Fig. 2(b), which optimizes resonant network symmetry for efficient power transmission and stable output.

B. Full Bridge Plus Half Bridge Mode

In FHB mode, the primary side switches form a full-bridge inverter. The switches in each bridge arm conduct complementarily at a 50% duty cycle: S_1 and S_4 turn ON together, as do S_2 and S_3. As depicted in Fig. 3(a), the first resonant network functions as a traditional full-bridge LLC resonant converter, while the second resonant network operates as a traditional half-bridge

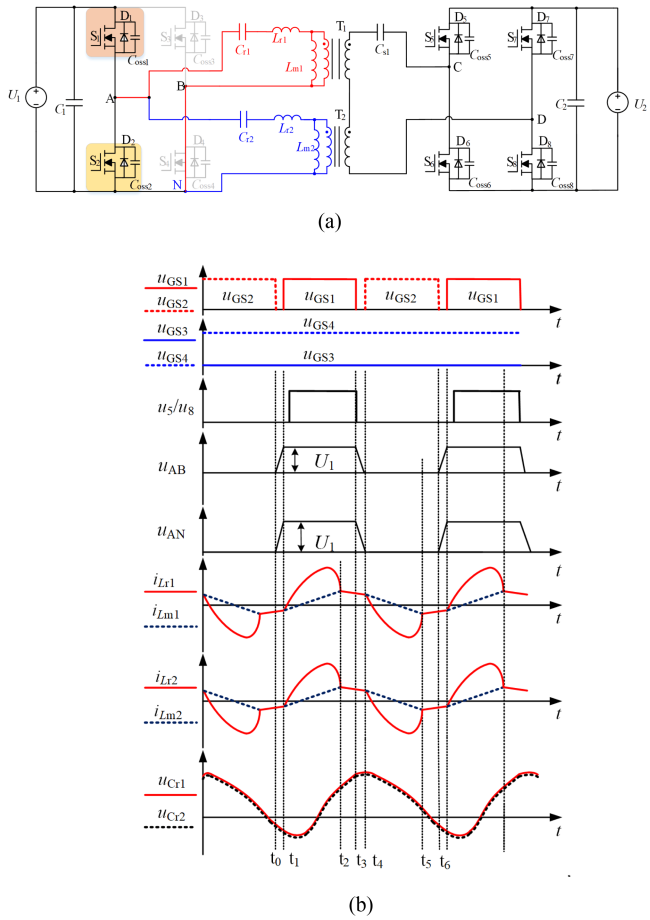

Fig. 2. Converter operates in DHB mode. (a) Equivalent circuit. (b) Main waveforms.

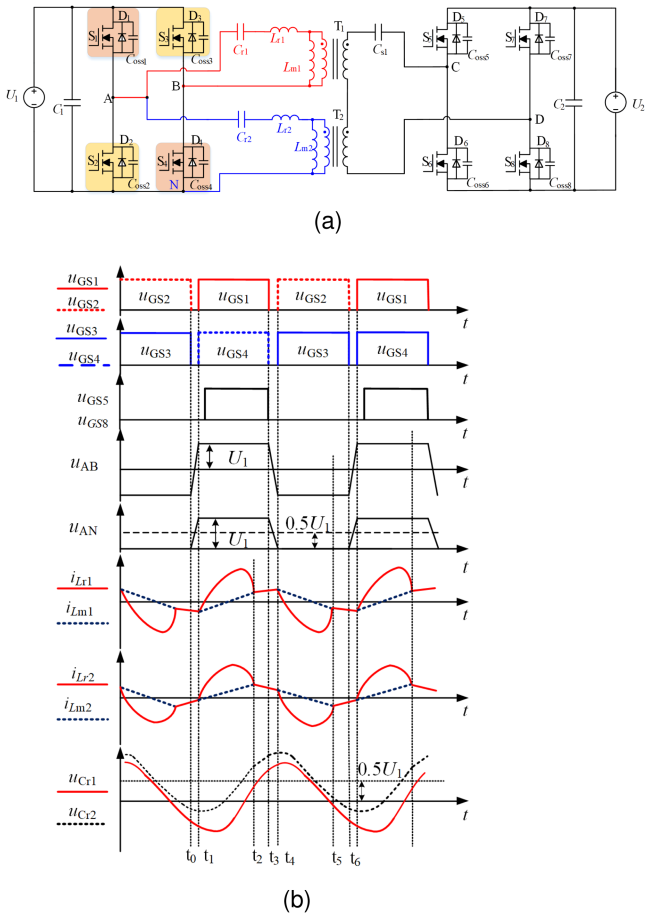

Fig. 3. Converter operates in FHB mode. (a) Equivalent circuit. (b) Main waveforms.

LLC resonant converter. The main operating waveforms for the converter in FHB mode are illustrated in Fig. 3(b).

C. Dual Voltage Doubling Circuit Mode

In DV mode, the secondary-side switches S_5–S_8 form a full-bridge inverter: the switches in each bridge arm conduct complementarily with a 50% duty cycle, where S_5 and S_8 are turned ON simultaneously, and S_6 and S_7 are turned ON simultaneously. The blocking capacitor C_{s1} is used to prevent dc bias in the transformers. On the primary side, switches S_1 and S_2 operate with synchronous rectification technology, while S_3 remains in the OFF state and S_4 remains in the ON state. The two resonant networks and the filter capacitor together form a voltage-doubling rectifier, which makes the entire circuit equivalent to two parallel half-bridge *LC* resonant converters, as illustrated in Fig. 4.

State 1 $[t_0, t_1]$: At instant t_0, switches S_6 and S_7 turn OFF, and the circuit enters the dead time. At this moment, the secondary-side transformer current i_s is negative, and the circuit operates in an over-resonant state. The resonant current drops rapidly to the magnetizing current; subsequently, the magnetizing current discharges the parasitic capacitances C_{oss5} and C_{oss8}, while charging the parasitic capacitances C_{oss6} and C_{oss7}, thereby creating the necessary conditions for the ZVS turn-ON of S_5 and S_8. On the primary side, switch S_2 remains OFF.

State 2 $[t_1, t_2]$: By instant t_1, the magnetizing current has charged C_{oss6} and C_{oss7} to the battery voltage U_2, and discharged C_{oss5} and C_{oss8} to zero, completing the charge-discharge process of the parasitic capacitances. During this period, i_s decreases sinusoidally and flows through the body diodes D_5 and D_8, which reduces the drain-source voltage of S_5 and S_8 to zero, enabling their ZVS turn ON.

State 3 $[t_2, t_3]$: At instant t_2, S_5 and S_8 achieve ZVS turn-ON, and i_s begins to increase. The magnetizing inductors L_{m1} and L_{m2} are clamped to U_2, thus exiting the resonant state (with their currents i_{Lm1} and i_{Lm2} rising linearly). Meanwhile, the resonant pairs L_{r1}, C_{r1} and L_{r2}, C_{r2} start to resonate, resulting in a sinusoidal i_s; energy is transferred from the secondary side to the primary side through the resonant tank. On the primary side, switch S_1 remains OFF.

D. Single Voltage Doubling Circuit Mode

In SV mode, the converter's circuit configuration is shown in Fig. 5. Secondary switches S_5-S_8 form a full-bridge inverter: each arm's two switches conduct complementarily with 50% duty cycle, with S_5/S_8 and S_6/S_7 turning ON simultaneously. Blocking capacitor C_{s1} prevents transformer dc bias. Primary

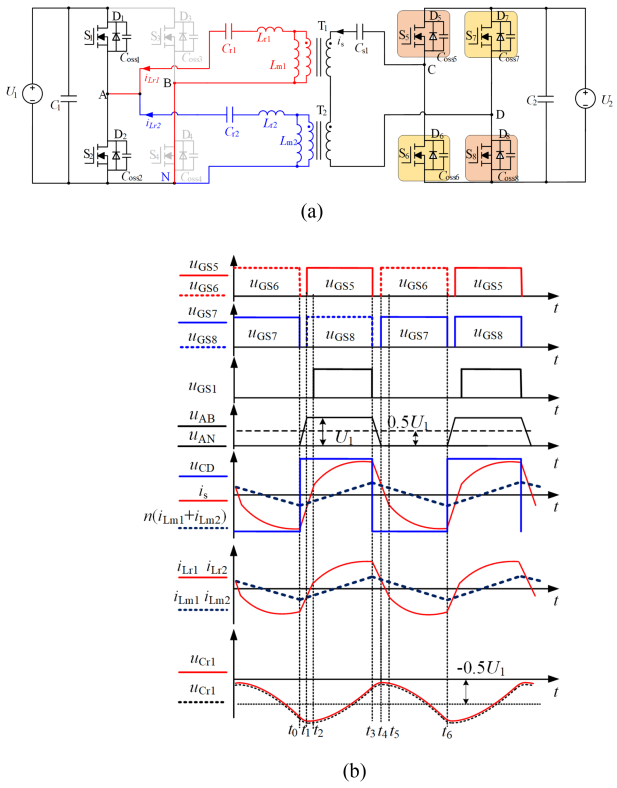

Fig. 4. Circuit topology in DV mode. (a) Equivalent circuit. (b) Main waveforms.

switches S_1-S_4 receive gate signals activate or deactivate: the first resonant network forms an LLC resonant converter, equivalent to a conventional full-bridge *LC* resonant converter, while the second resonant network and filter capacitor form a dual voltage-doubling rectifier.

State 1 [t_0, t_1]: At t_0, $S_6$and S_7 turn OFF, entering dead time. Secondary transformer current i_s is negative, and the circuit is in over-resonant state. Resonant current drops rapidly to magnetizing current, which discharges S_5 andS_8's parasitic capacitances $C_{oss5}$and C_{oss8} and charges S_6's andS_7's C_{oss6} andC_{oss7}—preparing for S_5andS_8 ZVS turn-ON. Primary-side S_2 and S_3 are open.

State 2 [t_1, t_2]: By t_1, magnetizing current charges $C_{oss6}$and C_{oss7} to U_2 and discharges C_{oss5} andC_{oss8} to zero, completing parasitic capacitance charge and discharge. i_s decreases sinusoidally and flows through $S_5$and S_8 body diodes D_5 andD_8, reducing their drain-source voltage to zero—establishing conditions for S_5 andS_8 ZVS turn-ON.

State 3 [t_2, t_3]: At t_2, $S_5$and S_8 achieve ZVS turn-ON; i_s increases. Magnetizing inductors L_{m1} andL_{m2} are clamped to U_2, exiting resonance (currents i_{Lm1}andi_{Lm2} rise linearly). L_{r1},C_{r1} and L_{r2},C_{r2} resonate, making i_s sinusoidal; energy transfers from secondary to primary via the resonant tank. Primary-side S_1 and S_4 are open.

III. Characteristic Analysis of the Proposed Converter

This article adopts the fundamental harmonic analysis (FHA) method to analyze the DBLLC resonant converter. Given that

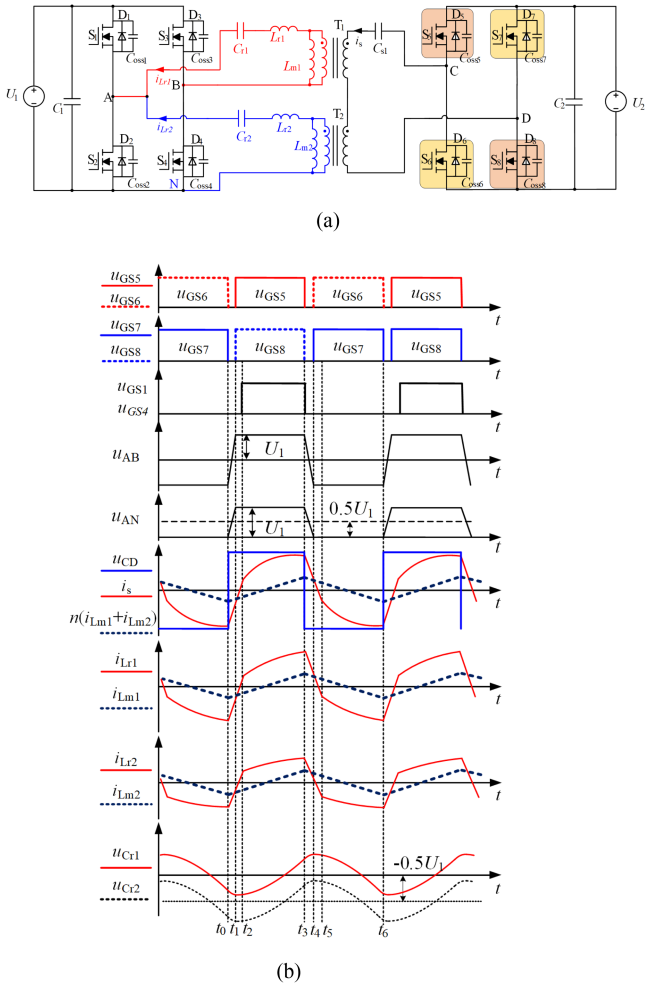

Fig. 5. Circuit topology in SV mode. (a) Equivalent circuit. (b) Main waveforms.

the proposed DBLLC converter has two resonant networks with identical parameters and shares switches S_1–S_4, it can be analyzed using an equivalent circuit approach.

The two resonant networks are parallel-connected on the transformer primary side, while their secondary voltages are series-connected before entering the rectifier circuit—enabling component combination. The equivalent parameters are derived as follows: equivalent resonant inductance $L_r = 0.5L_{r1} = 0.5L_{r2}$, equivalent resonant capacitance $C_r = 2C_{r1} = 2C_{r2}$, equivalent transformer magnetizing inductance $L_m = 0.5L_{m1} = 0.5L_{m2}$, and equivalent turns ratio of the two ideal transformers $n = 0.5n_1 = 0.5n_2$. Here, u_{s1} and u_{s2} represent the secondary voltages of the transformers in the first and second resonant circuits, respectively, and u_{in} denotes the input voltage.

A. Analysis of the Forward Voltage Gain of the Converter

In FHB mode, u_{AB} has no dc offset. However, u_{AN} has a dc offset of $0.5U_{in}$, and the entire dc offset voltage is borne by C_{r2}; thus, u_{AN} can be equivalently expressed as $u_{AN} = \pm 0.5U_{in}$. During the converter operation from t_0 to t_2, ignoring the dead time effect from t_0 to t_1, the state variables in the full-bridge

resonant network can be represented as

$$\begin{cases} C_{\mathrm{r1}}\frac{\mathrm{d}u_{\mathrm{Cr1}}}{\mathrm{d}t} = i_{\mathrm{Lr1}} \\ L_{\mathrm{r1}}\frac{\mathrm{d}i_{\mathrm{Lr1}}}{\mathrm{d}t} = U_{\mathrm{in}} - u_{\mathrm{Cr1}} - n_1 u_{\mathrm{s1}} \\ L_{\mathrm{m1}}\frac{\mathrm{d}i_{\mathrm{m1}}}{\mathrm{d}t} = n_1 u_{\mathrm{s1}}. \end{cases} \tag{1}$$

Similarly, the state variables in the half-bridge resonant network during the time interval t_0 to t_2 can be represented as

$$\begin{cases} C_{\mathrm{r2}}\frac{\mathrm{d}u'_{\mathrm{Cr2}}}{\mathrm{d}t} = i_{\mathrm{Lr2}} \\ L_{\mathrm{r2}}\frac{\mathrm{d}i_{\mathrm{Lr2}}}{\mathrm{d}t} = 0.5U_{\mathrm{in}} - u'_{\mathrm{Cr2}} - n_2 u_{\mathrm{s2}} \\ L_{\mathrm{m2}}\frac{\mathrm{d}i_{\mathrm{m2}}}{\mathrm{d}t} = n_2 u_{\mathrm{s2}} \end{cases} \tag{2}$$

where the $u'_{\mathrm{Cr2}} = u_{Cr2} - 0.5U_{in}$.

When the converter operates between t_2 and t_3, the resonant current and the magnetizing current can be considered to always remain consistent. The state variable of the full-bridge resonant network during t_2 to t_3 can be represented as

$$\begin{cases} C_{\mathrm{r1}}\frac{\mathrm{d}u_{\mathrm{Cr1}}}{\mathrm{d}t} = i_{\mathrm{Lr1}} \\ (L_{\mathrm{r1}} + L_{\mathrm{m1}})\frac{\mathrm{d}i_{\mathrm{Lr1}}}{\mathrm{d}t} = U_{\mathrm{in}} - u_{\mathrm{Cr1}} \\ i_{\mathrm{m1}} = i_{\mathrm{Lr1}}. \end{cases} \tag{3}$$

Similarly, during the period t_2 to t_3, the state variable in the half-bridge resonant network can be represented as

$$\begin{cases} C_{\mathrm{r2}}\frac{\mathrm{d}u'_{\mathrm{Cr2}}}{\mathrm{d}t} = i_{\mathrm{Lr2}} \\ (L_{\mathrm{r2}} + L_{\mathrm{m2}})\frac{\mathrm{d}i_{\mathrm{Lr2}}}{\mathrm{d}t} = 0.5U_{\mathrm{in}} - u'_{\mathrm{Cr2}} \\ i_{\mathrm{m2}} = i_{\mathrm{Lr2}}. \end{cases} \tag{4}$$

By adding (3) and (4), the equivalent state variable expression for the converter operating during the interval from t_2 to t_3 can be obtained, which is denoted as

$$\begin{cases} C_{\mathrm{r}}\frac{\mathrm{d}u_{\mathrm{Cr}}}{\mathrm{d}t} = i_{\mathrm{Lr}} \\ (L_{\mathrm{r1}} + L_{\mathrm{m1}})\frac{\mathrm{d}i_{\mathrm{Lr1}}}{\mathrm{d}t} + (L_{\mathrm{r2}} + L_{\mathrm{m2}})\frac{\mathrm{d}i_{\mathrm{Lr2}}}{\mathrm{d}t} = 1.5U_{\mathrm{in}} - u_{\mathrm{Cr}} \\ i_{\mathrm{m}} = i_{\mathrm{m1}} + i_{\mathrm{m2}} = i_{\mathrm{Lr1}} + i_{\mathrm{Lr2}} = i_{\mathrm{Lr}} \end{cases} \tag{5}$$

where the $u_{Cr} = (u_{Cr1} + u'_{\mathrm{Cr2}})$.

In the FHB mode, the voltage gain expression can be written as

$$M_{FHB} = \frac{nU_o}{U_{in}} \frac{1.5}{\sqrt{\left[1 + \frac{1}{k}\left(1 - \frac{1}{f_n^2}\right)\right]^2 + \left(f_n - \frac{1}{f_n}\right)^2 Q^2}}. \tag{6}$$

In the equation, the normalized switching frequency f_n, the inductance ratio k, the ac equivalent resistance R_{ac}, the characteristic impedance of the resonant network Z_r, and the quality factor Q can be expressed as

$$\begin{cases} f_{\mathrm{n}} = f_{\mathrm{s}}/f_{\mathrm{r}} \\ k = L_{\mathrm{m}}/L_{\mathrm{r}} \\ R_{\mathrm{ac}} = 8n^2 R_o/\pi^2 \\ Z_{\mathrm{r}} = \sqrt{L_{\mathrm{r}}/C_{\mathrm{r}}} \\ Q = Z_{\mathrm{r}}/R_{\mathrm{ac}}. \end{cases} \tag{7}$$

Similarly, the expression for normalized voltage gain in DHB mode can be obtained

$$M_{\mathrm{DHB}} = \frac{nU_{\mathrm{o}}}{U_{\mathrm{in}}} \frac{1}{\sqrt{\left[1 + \frac{1}{k}\left(1 - \frac{1}{f_{\mathrm{n}}^2}\right)\right]^2 + \left(f_{\mathrm{n}} - \frac{1}{f_{\mathrm{n}}}\right)^2 Q^2}}. \tag{8}$$

B. Analysis of Reverse Voltage Gain of the Converter

In DV mode, the converter uses a full-bridge input configuration. The resonant tank input voltage is a square wave with amplitude $\pm U_2$, while the rectifier-side output voltage is a square wave with amplitude $\pm U_1/2$. Thus, the fundamental rms values of the input and output voltages satisfy

$$\begin{cases} U_{2,FHA} = \frac{2\sqrt{2}}{\pi} U_2 \\ U_{1,FHA} = \frac{2\sqrt{2}}{\pi} U_1 \end{cases} \tag{9}$$

$U_{2,FHA}$, $U_{1,FHA}$ are the fundamental effective values of the input voltage and output voltage, respectively.

The current of the rectifier I_{rec} is related to the output current I_1 by

$$I_1 = \frac{2}{T_S}\int_0^{\frac{T_s}{2}} \left|\sqrt{2I_{\mathrm{rec}}\sin(\omega t - \varphi)}\right| \mathrm{d}t = \frac{2\sqrt{2}I_{\mathrm{rec}}}{\pi}. \tag{10}$$

In DV mode, the ac equivalent resistance $R_{o,ac}$ at the rectifier side of the converter is defined as

$$R_{o,ac} = \frac{U_{1,FHA}}{I_{\mathrm{rec}}} = \frac{4U_1}{\pi^2 I_1} = \frac{4}{\pi^2} R_0. \tag{11}$$

Equivalent resistance of primary side ac

$$R_{ac} = n^2 R_{o,ac} = \frac{4n^2}{\pi^2} R_0. \tag{12}$$

The transfer function $H(s)$ of the equivalent circuit can be expressed as

$$H_{DV}(S)_{s=j\omega} = \frac{U_{1,FHA}(S)}{U_{2,FHA}(S)} = \frac{R_{ac}}{sL_r + \frac{1}{sC_r} + R_{ac}}. \tag{13}$$

In DV mode, the resonant frequency f_r, characteristic impedance Z_1 of the equivalent resonant network, quality factor Q, and switching frequency f_n are defined as

$$\begin{cases} f_{\mathrm{n}} = f_{\mathrm{s}}/f_{\mathrm{r}} \\ f_r = \frac{1}{2\pi\sqrt{L_r C_r}} \\ R_{\mathrm{ac}} = 8n^2 R_o/\pi^2 \\ Z_1 = \sqrt{L_{\mathrm{r}}/C_{\mathrm{r}}} \\ Q = Z_1/n^2 R_{\mathrm{o,ac}}. \end{cases} \tag{14}$$

After sorting, it can be obtained

$$H_{DV}(s)_{s=j\omega} = \frac{U_{1,FHA}(s)}{U_{2,FHA}(s)} = \frac{1}{1 + \frac{1}{k}\left(1 - \frac{1}{f_n{}^2}\right) + jQ\left(f_n - \frac{1}{f_n}\right)}. \tag{15}$$

Therefore, the normalized voltage gain M_{DV} in DV mode can be expressed as

$$M_{DV} = \frac{1}{\sqrt{1 + \left(f_n * 2Q - \frac{2Q}{f_n}\right)^2}}. \tag{16}$$

In SV mode, the energy transfer path is the same as in DV mode: energy is first converted by a full-bridge inverter and transferred to the primary side via the transformer. Thus, the resonant tank input voltage is a square wave with amplitude U_2. The key difference is the rectification configuration: the first resonant network adopts full-bridge rectification, while the second uses

TABLE I
DESIGN PARAMETERS OF THE PROTOTYPE

Items	Parameters
Input voltage(U_{in})	400 V
Output voltage (U_o)	250-500 V
Output power(P_o)	2.5 kW
Resonant frequency(f_r)	100 kHz

voltage-doubler rectification. As a result, the secondary-side output voltage amplitudes of the two resonant networks are U_1 and a pulsating square wave (0 to U_1), respectively.

In SV mode, the ac equivalent resistance at the rectifier port of the first resonant network ($R_{o1,ac}$) and that of the second resonant network ($R_{o2,ac}$) can be expressed as

$$\begin{cases} R_{o1,ac} = \frac{U_{2,FHA}}{I_{rec}} = \frac{8U_2}{\pi^2 I_2} = \frac{8}{\pi^2} R_0 \\ R_{o2,ac} = \frac{U_{2,FHA}}{I_{rec}} = \frac{4U_2}{\pi^2 I_2} = \frac{4}{\pi^2} R_0. \end{cases} \tag{17}$$

In SV mode, the equivalent ac resistance on the primary side of the first resonant network R_{ac1} and that of the second resonant network R_{ac2} can be expressed as

$$\begin{cases} R_{ac1} = n^2 R_{o1,ac} = \frac{8n^2}{\pi^2} R_0 \\ R_{ac2} = n^2 R_{o2,ac} = \frac{4n^2}{\pi^2} R_0. \end{cases} \tag{18}$$

In SV mode, the quality factors of the first and second resonant networks, denoted as Q_1 and Q_2, respectively, can be expressed as

$$\begin{cases} Q_{ac1} = \frac{Z_1}{n^2 R_{o,ac}} = \frac{Z_1 \pi^2}{8n^2 R_0} \\ Q_{ac2} = \frac{Z_1}{n^2 R_{o,ac}} = \frac{Z_1 \pi^2}{4n^2 R_0}. \end{cases} \tag{19}$$

The normalized voltage gain M_{SV} in SV mode can be expressed as

$$M_{SV} = \frac{0.5}{\sqrt{1 + (f_n * 2Q - \frac{2Q}{f_n})^2}} + \frac{0.5}{\sqrt{1 + (f_n Q - \frac{Q}{f_n})^2}}. \tag{20}$$

IV. DESIGN AND CONTROL OF THE PROPOSED CONVERTER

A. Design of Circuit Parameters

The design specifications of the proposed converter are given in Table I. The key to realizing ZVS for a switch is that the turn-OFF current I_r charges and discharges the switch's output capacitance C_{oss} during dead time. Thus, a sufficiently large current must exist in dead time to ensure full charge-discharge of C_{oss}. Based on the law of conservation of charge can derive

$$I_r T_d > 2 C_{oss} U_1. \tag{21}$$

In DHB mode, the resonant current i_r is approximately equal to the peak magnetizing current

$$i_{r1,p} = i_{r2,p} = \frac{nU_o}{4 f_r L_m}. \tag{22}$$

Therefore, the constraint conditions for the excitation inductance are

$$L_m < \frac{nU_2 T_d}{8U_1 C_{oss} f_r}. \tag{23}$$

The limiting conditions for the excitation inductance required for achieving soft-switching in the DHB mode and the FHB mode are

$$L_{m,DHB} < \frac{T_d}{16 C_{oss} f_r} \tag{24}$$

$$L_{m,FHB} < \frac{T_d}{8 C_{oss} f_r}. \tag{25}$$

From (24) and (25), the excitation inductance L_m required for soft switching in DHB mode is smaller. Thus, (24) is selected as the constraint condition for realizing the converter's soft switching.

At the resonant frequency, the designed voltages for DHB and FHB modes are 250 and 375 V, respectively, with 375 V set as the transition voltage between the two modes. When operating in DHB mode, the circuit is equivalent to a dual-phase half-bridge LLC converter. Based on the input and output voltages of FHB mode at the resonant frequency, the turns ratios n_1 and n_2 of the two transformers can be derived as follows:

$$n = \frac{U_{\text{in}}}{U_{\text{o}}} = \frac{400}{250} = 1.6. \tag{26}$$

In FHB mode, the converter only needs a voltage gain of 1.33 to cover the 375–500 V range; thus, the key design focus is enabling DHB mode to achieve a voltage gain of 1.5 within a narrow frequency range. A smaller k broadens the voltage gain range but increases circulating and conduction losses, lowering efficiency. In contrast, a larger k reduces resonant rms current and conduction losses but narrows the gain range—so a larger k is preferred to improve transformer efficiency while meeting gain requirements.

Additionally, the voltage gain curve decreases as the quality factor Q increases, which may fail to meet gain requirements; however, a smaller Q reduces impedance, leading to larger circulating currents and lower efficiency. Hence, a larger Q is desirable to satisfy both gain and efficiency needs. As derived in Section III, the gain curves for forward and reverse operations are obtained, as shown in Fig. 6. For forward operation, Fig. 6(a) shows that the DHB mode covers the secondary voltage range of $U_2 = 250 - -375$ V. As the normalized frequency f_n decreases from 1.0 to 0.63, the normalized gain M rises from approximately 1–1.5. When $U_2 = 375$ V, the switching frequency point f_n jumps to 1.0 and the circuit enters the FHB mode. The FHB mode covers $U_2 = 375 - -500$ V, as f_n drops from 1 to 0.68, M increases to 2 ($U_2 = 500$ V), which is consistent with the experimental waveforms of the forward mode in Figs. 9 and 10.

For backward operation, Fig. 6(b) shows that the SV mode covers $U_2 = 375 - -500$ V. As f_n decreases from 2.0 to 1.0, M increases from about 0.78 to 0.9375. When $U_2 = 375$ V, the switching frequency point f_n jumps to 2.0 and the circuit enters the DV mode. The DV mode covers $U_2 = 250 - -375$ V, as f_n decreases from 2.0 back to 1.0, M increases from 0.66 to 1, with the primary voltage U_1 stably maintained at 400 V. This

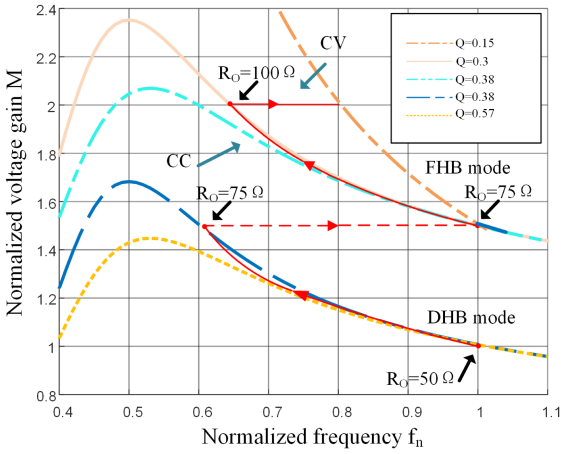

(a)

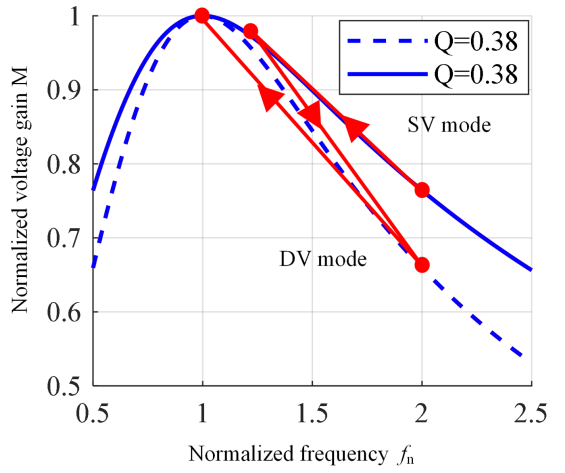

(b)

Fig. 6. Voltage gain curves. (a) Forward voltage gain curves. (b) Backward voltage gain curves.

TABLE II
PARAMETERS OF THE DBLLC CONVERTER

Parameters	Notation	Value
Primary side voltage	U_{in}	400 V
Secondary side voltage	U_o	250–500 V
Rated output power	P_o	2.5 kW
Resonant capacitance	C_{r1},C_{r2}	54 nF
Resonant inductance	L_{r1},L_{r2}	47μH/PQ2620
Magnetizing inductance	L_{m1},L_{m2}	197μH
Core of transformer	T_1	PQ4040
Core of transformer	T_2	PQ3535
Turns ratio	n_1,n_2	1.6
MOSFET switches	S_1-S_8	S1M075120D2
Switching parasitic capacitance	C_{oss}	64pF
Output capacitor	C_1,C_2	220μF*2
Resonant frequency	f_r	100 kHz
Switching frequency	f_s	62-100-200 kHz

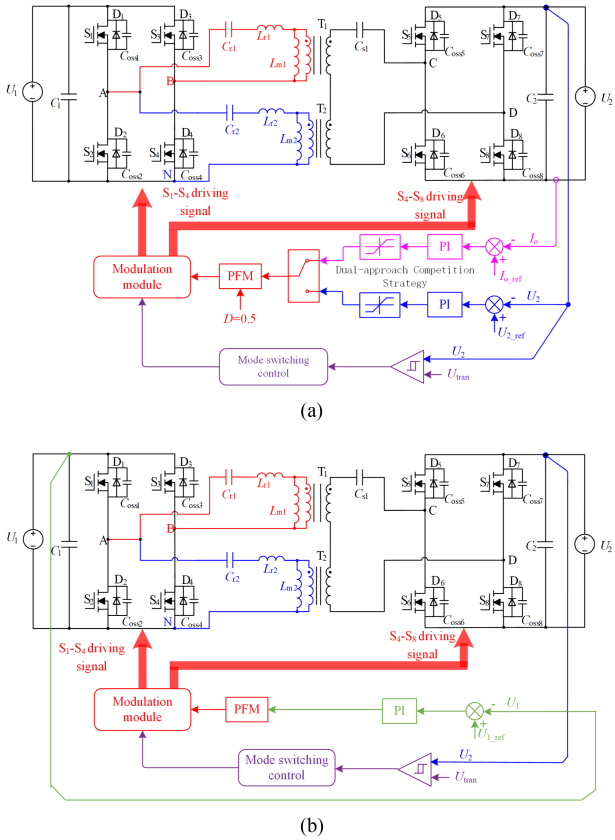

(a)

(b)

Fig. 7. Variable mode bidirectional converter system control diagram. (a) Forward control block diagram. (b) Backward control block diagram.

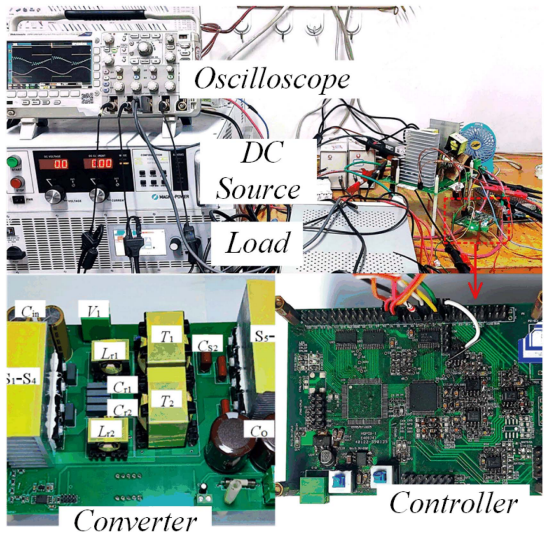

Fig. 8. Experimental platform of the DBLLC converter.

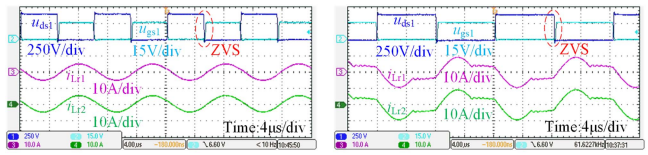

(a) (b)

Fig. 9. Waveforms in forward DHB mode. (a) U_2 =250 V, P_o =1250 W. (b) U_2 =375 V, P_o =1875 W.

TABLE III
COMPARISON OF THE PROPOSED AGAINST EXISTING CONVERTERS

References	Converter in [6]	Converter in [11]	Converter in [19]	Converter in [20]	Converter in [22]	Proposed
Number of switches	10	8	12	8	8	8
Modulation	PSM	PSM	PFM	PFM	PFM+PSM	PFM
Input voltage	100-400V	500V	400V	400V	400V	400V
Output voltage	400V	250-500V	150-500V	50-450V	250-450V	250-500V
Output power	1kW	1kW	0.5kW	0.3kW	3.3kW	2.5kW
Peak efficiency	97.9%	97%	96.8%	94.3%	97.3%	98%

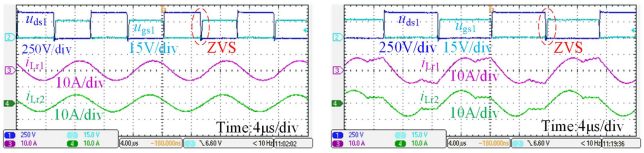

(a) (b)

Fig. 10. Waveforms in forward FHB mode. (a) U_2 =375 V, P_o =1875 W. (b) U_2 =500 V, P_o =2500 W.

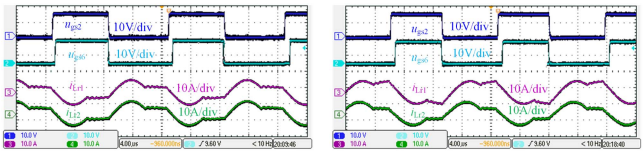

(a) (b)

Fig. 11. Synchronous rectification under forward operation. (a) DHB mode $U_2 = 375$ V, $P_o = 1875$ W. (b) FHB mode $U_2 = 500$ V, $P_o = 2500$ W.

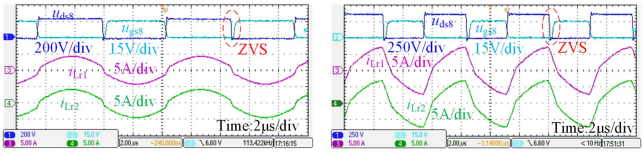

(a) (b)

Fig. 12. Waveforms in backward DV mode. (a) $U_2 = 250$ V, $P_o = 1250$ W. (b) $U_2 = 375$ V, $P_o = 1875$ W.

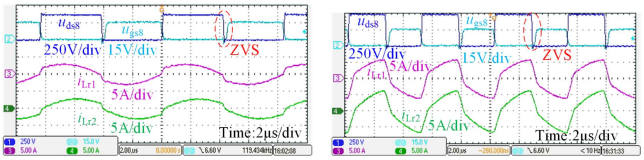

(a) (b)

Fig. 13. Waveforms in backward SV mode. (a) $U_2 = 375$ V, $P_o = 1875$ W. (b) $U_2 = 500$ V, $P_o = 2500$ W.

is consistent with the experimental waveforms of the backward mode in Figs. 12 and 13.

B. Design of Control Strategy

This article focuses on constant current (CC) and constant voltage (CV) charging technologies. For forward operation, the converter adopts a dual-loop competitive control strategy integrating current and voltage loops, while PI control is used for reverse operation; its control flow is shown in Fig. 7. Taking forward operation as an example: the system first operates in CC mode, switching to CV mode when voltage reaches 500 V, continuing until current stabilizes at the final value $I_o = 1$ A to end charging. Specifically, the voltage loop compares secondary-side voltage U_2 with the 500 V target, with deviation processed by a PI regulator to generate a frequency adjustment signal, regulating primary and secondary switching frequencies to meet forward voltage gain requirements. The current loop compares secondary-side current I_2 with rated current, with deviation also processed by a PI regulator for frequency adjustment. The system selects the smaller adjustment signal for operation, keeping the other loop inactive: when the set voltage exceeds actual output and set current is lower than actual output, the current loop regulates current, conversely, the voltage loop regulates voltage. When secondary voltage rises to 375 V, mode switching is triggered from DHB to FHB. For reverse operation, a single-loop CV control is used: the voltage loop compares primary-side voltage U_1 with 400 V, with deviation processed by a PI regulator to adjust switching frequency for reverse gain requirements. When battery voltage drops to 375 V, primary operation switches from DV to SV mode.

The mode switching point for both directions is 375 V. For forward operation, core strategies include pretransition frequency calibration and dead-time coordination: as U_2 approaches 375 V (hysteresis upper threshold 378 V), the controller increases frequency from 63 to 100 kHz within 20 μ s to meet FHB mode gain. To prevent shoot-through and current spikes, S_3 switches from turn-OFF to 50% duty cycle during transition, with 200 ns dead time between its drive signal and S_1/S_2 signals. Post-transition, dual-loop control fine-tunes f_s within 1 μ s for smooth switching. For reverse operation, switching at $U_2 = 375$ V uses pre-enabling mode signals and preclamping resonant capacitor voltages: as U_2 approaches 375 V (hysteresis upper threshold 370 V), f_s adjusts to 150 kHz to smoothly transition u_{Cr1} to -0.5U_1; S_4 is turned ON 10 μs in advance via low-voltage soft start. Post-transition, f_s adjusts to the target within 20 μs for smooth switchover.

V. EXPERIMENTAL RESULT

To verify the practical applicability and operational effectiveness of the DBLLC converter, a 2.5 kW rated-power experimental platform was built. The platform features a 400 V dc bus voltage and a secondary-side voltage range of 250–500 V. A photograph of the experimental platform is shown in Fig. 8, and its configuration and component arrangement are detailed in Table II.

A. Forward Operation

The forward-mode experimental waveforms of the DBLLC converter are shown in Figs. 9 and 10, characterizing its operation under different conditions.

In DHB mode, when the secondary side outputs 250 V/5 A (f_s = 100 kHz) and 375 V/5 A (f_s = 63 kHz), the key waveforms are given in Fig. 9(a) and (b), respectively. Here, u_{gs1} and u_{ds1} denote the gate-source drive signal and drain-source voltage of S_1. The waveforms show S_1's drain-source voltage drops to zero before the gate-source voltage rises, confirming ZVS. In FHB mode, for secondary outputs 375 V/5 A (f_s = 100 kHz) and 500 V/5 A (f_s = 68 kHz), critical waveforms are in Fig. 10(a) and (b); u_{gs1} and u_{ds1} reflect S_1's drive and voltage states. Waveform analysis confirms ZVS is also achieved, showing consistent soft-switching across voltage ranges.

Notably, in DHB mode, resonant currents i_{r1} and i_{r2} have identical waveforms, indicating balanced current distribution. This symmetry ensures each transformer transmits half the total power, validating the dual-transformer equal power-sharing design. In FHB mode, transformer T_1 transmits 2/3 of total power and T_2 transmits 1/3, with ZVS realized for S_1–S_4.

Fig. 11 presents synchronous rectification waveforms in DHB and FHB modes. In DHB mode (secondary 375 V/5 A, f_s = 63 kHz), key waveforms are in Fig. 11(a); u_{gs2} and u_{ds6} are the gate-source signals of S_2 and S_6. The waveforms show S_6 turns ON/OFF synchronously with S_2 to achieve synchronous rectification. In FHB mode (secondary 500 V/5 A, f_s = 68 kHz), key waveforms are in Fig. 11(b); again, S_6 turns ON/OFF synchronously with S_2 for synchronous rectification.

B. Backward Operation

The converter's experimental waveforms in DV and SV modes are shown in Figs. 12 and 13, respectively, illustrating its performance under different operational modes.

In DV mode, for secondary outputs of 250 V/5 A (f_s = 100 kHz) and 375 V/5 A (f_s = 200 kHz), key waveforms are presented in Fig. 12(a) and (b). Here, u_{gs8} and u_{ds8} denote the gate-source drive signal and drain-source voltage of S_8; waveform analysis shows the gate-source voltage rises only after the drain-source voltage drops to zero, confirming ZVS for S_8. In SV mode, for secondary outputs of 375 V/5 A (f_s = 100 kHz) and 500 V/5 A (f_s = 200 kHz), critical waveforms are in Fig. 13(a) and (b); u_{gs8} and u_{ds8} reflect S_8's drive and voltage states. Results confirm ZVS is also achieved, demonstrating consistent soft-switching across configurations.

Notably, power distribution differs between modes: in DV mode, the two transformers share power equally (each carrying half the total power); in SV mode, T_1 transmits 2/3 of total power and T_2 1/3, an intentional design feature of SV mode. Importantly, switches S_5–S_8 achieve ZVS in both modes, verifying the soft-switching design's effectiveness across the entire topology.

Fig. 14 shows synchronous rectification waveforms in SV and DV modes. In SV mode (secondary input 375 V/5 A, f_s = 100 kHz), key waveforms are in Fig. 14(a); u_{gs8} and u_{ds1} are the gate-source signals of S_8 and S_1. The waveforms clearly show

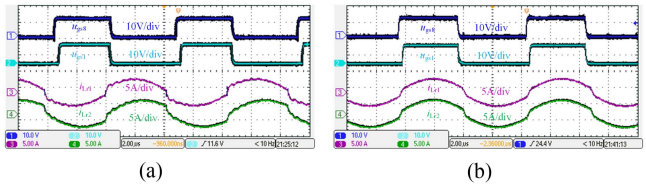

(a) (b)

Fig. 14. Synchronous rectification under reverse operation. (a) SV mode U_2 = 375 V, P_o = 1875 W. (b) DV mode U_2 = 250 V, P_o = 1250 W.

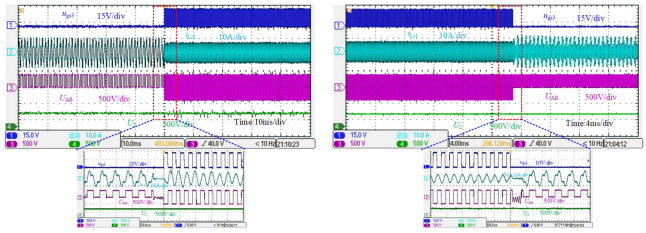

(a) (b)

Fig. 15. Transition waveforms in forward of U_2 = 375 V, P_o = 1875 W. (a) DHB mode to FHB mode. (b) FHB mode to DHB mode.

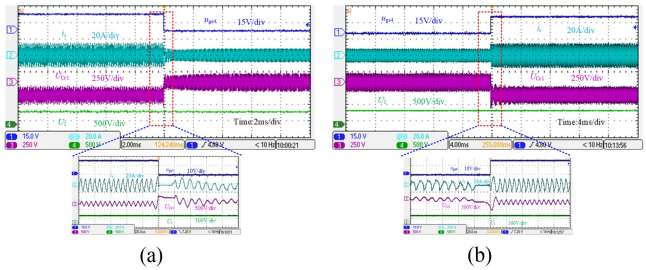

(a) (b)

Fig. 16. Transition waveforms in backward of U_2 = 375 V,P_o = 1875 W. (a) DV mode to SV mode. (b) SV mode to DV mode.

S_1 turns ON/OFF synchronously with S_8 to achieve synchronous rectification.

Figs. 15 and 16 show the DBLLC converter's mode transition waveforms. During DHB to FHB and FHB to DHB transitions, the drive signal u_{GS3} of S_3 changes: S_3 is OFF in DHB mode, while it generates a 50% duty cycle square wave in FHB mode. Though switching frequency and inductor currents i_{r1}, i_{r2} change during transition, secondary voltage U_2 stays at 375 V. The first resonant network's input voltage u_{AB} is a 0–U_1 square wave in DHB mode and a $\pm$ U_1 square wave in FHB mode. All variables operate within safe limits, with no overshoot or undershoot.

Fig. 16(a) and (b) shows DV to SV and SV to DV transition waveforms, respectively. The drive signal u_{GS4} of S_4 changes: S_4 is ON in DV mode and OFF in SV mode. During transition, switching frequency and secondary current i_s amplitude change, but primary voltage U_1 remains at 400 V. The first resonant network's resonant capacitor voltage u_{cr1} is a 0–U_1 square wave in DV mode and a $\pm$ U_1 square wave in SV mode. All variables are within safe limits, with no overshoot or undershoot. In summary, the proposed converter achieves smooth mode transitions.

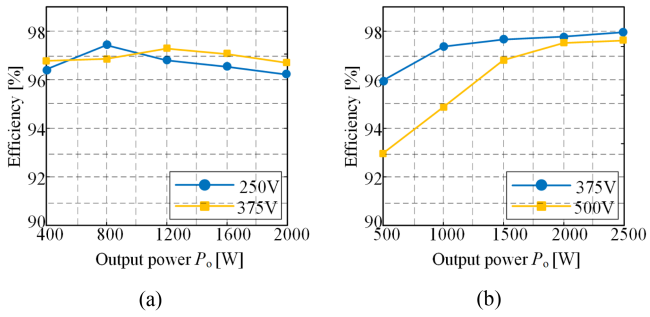

Fig. 17. Efficiency curve of DBLLC converter in forward. (a) DHB mode. (b) FHB mode.

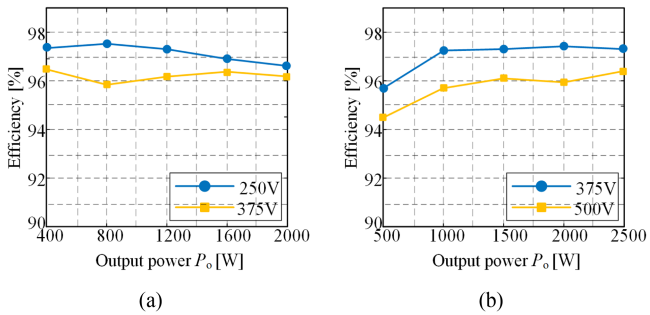

Fig. 18. Efficiency curve of DBLLC converter in backward. (a) DV mode. (b) SV mode.

C. Analysis and Comparison of Platform Efficiency

During the forward operation of the converter with synchronous rectification, the efficiency curves of the two modes are shown in Fig. 17. In the DHB mode, the base efficiency of the converter is around 96.7%, and the efficiency decreases more gradually as the output power increases. This is because synchronous rectification significantly reduces the on-state loss under large current conditions. The higher the output voltage at constant power, the lower the corresponding current, and the advantage of synchronous rectification's on-state loss becomes more obvious, resulting in better efficiency performance; conversely, at low voltage and high current output, the efficiency is slightly lower. In FHB mode, synchronous rectification further raises the converter's efficiency to over 97%. Notably, lower output voltage brings the switching frequency closer to the resonant frequency: at this point, not only is the resonant network loss minimized, but the timing matching of synchronous rectification is also optimized, thus achieving the highest efficiency. Additionally, the converter's efficiency remains relatively low under light loads. This is because the LLC resonant converter must increase its operating frequency to stabilize the voltage, and switching loss becomes dominant at high frequencies; while synchronous rectification can reduce on-state loss, its effect on mitigating switching loss is limited.

Fig. 18 presents the efficiency curves of the converter with synchronous rectification in reverse operation for DV and SV modes, reflecting further optimized energy conversion performance during bidirectional operation. In DV mode, at low output voltages, switching frequency is close to resonant frequency—minimizing reactive power loss to the greatest extent. Meanwhile, primary-side synchronous rectification reduces conduction-phase energy loss, raising the converter's peak efficiency to 97.5% and improving energy transmission performance. However, at an output voltage of 375 V, resonant-related switching frequency increases significantly, making switching loss dominant and causing efficiency to drop. In SV mode, at low output voltages, frequency is also near the resonant point, and synchronous rectification timing is more in phase with resonant current—minimizing conduction loss and further boosting efficiency to 97.4%. As output voltage increases, switching frequency deviates from the resonant point, increasing switching loss and leading to a downward efficiency trend.

Table III presents a comparison between the proposed topology and reported converters. As shown in Table III, the DBLLC converter has a small number of switches, which reduces the cost of the converter. The DBLLC converter expands the voltage range.

VI. Conclusion

This article introduces a variable mode bidirectional LLC resonant converter with dual-resonant branches, which enables mode switching between DHB and FHB during forward power transfer, and between DV and SV modes during reverse operation through drive signal adjustment. All operational modes employ variable frequency modulation, streamlining the control strategy and facilitating wide gain range operation within a relatively narrow switching frequency range while supporting bidirectional power flow. A 2.5 kW experimental platform was developed to validate the design. Test results demonstrate that the converter achieves full range soft switching across all voltage levels, ensures smooth start-up without inrush current, and avoids current transients during mode transitions. The platform achieves a peak efficiency of 98% in forward operation and 97.5% in reverse operation, showcasing its high efficiency performance across bidirectional power transfer.

References

[1] R. Zaino, V. Ahmed, A. M. Alhammadi, and M. Alghoush, "Electric vehicle adoption: A comprehensive systematic review of technological, environmental, organizational and policy impacts," *World Electric Veh. J.*, vol. 15, no. 8, Aug. 2024, Art. no. 375.

[2] J. Bouanani, M. Yessef, and A. Lagrioui, "Toward efficient energy management in electric and hybrid vehicles: Progress, prospects and emerging trends of hybrid storage systems," in *Proc. 17th Int. Conf. Electron.*, Comput. Artif. Intell., Targoviste, Romania, 2025, pp. 1–6.

[3] C. Bai, B. Han, B.-H. Kwon, and M. Kim, "Highly efficient bidirectional series-resonant dc/dc converter over wide range of battery voltages," *IEEE Trans. Power Electron.*, vol. 35, no. 4, pp. 3636–3650, Apr. 2020.

[4] Y. Wang, M. Zhang, B. Chen, M. Chen, C. Chen, and C. Che, "A novel bidirectional TLCT resonant dc-dc converter with wide voltage range," in *Proc. IEEE Energy Convers. Congr. Expo.*, 2022, pp. 1–6.

[5] N. Patel, L. A. C. Lopes, A. K. Rathore, and V. Khad-kikar, "High-efficiency single-stage single-phase bidirectional PFC converter for plug-in EV charger," *IEEE Trans.Transport. Electrific.*, vol. 10, no. 3, pp. 5636–5649, Sep. 2024.

[6] Q. Zhao, Y. Gao, H. Ding, Z. Wu, X. Li, and D. Wang, "Bidirectional hybrid dc–dc resonant converter with wide voltage gain range," *IEEE Trans. Ind. Electron.*, vol. 72, no. 5, pp. 4721–4730, May 2025.

[7] I.-O. Lee and G.-W. Moon, "The k-Q analysis for an LLC series resonant converter," *IEEE Trans. Power Electron.*, vol. 29, no. 1, pp. 13–16, Jan. 2014.

[8] L. A. D. Ta, N. D. Dao, and D.-C. Lee, "High-efficiency hybrid LLC resonant converter for on-board chargers of plug-in electric vehicles," *IEEE Trans. Power Electron.*, vol. 35, no. 8, pp. 8324–8334, Aug. 2020.
[9] D. Chen, J. Deng, M. Li, Z. Wang, and S. Wang, "An enhanced dual active bridge converter with full domain ZVS by utilizing a simple segment control for wide voltage range applications," *IEEE Trans. Ind. Electron.*, vol. 69, no. 7, pp. 6817–6827, Jul. 2022.
[10] S. Khan, D. Sha, X. Jia, and S. Wang, "Resonant LLC dc–dc converter employing fixed switching frequency based on dual-transformer with wide input-voltage range," *IEEE Trans. Power Electron.*, vol. 36, no. 1, pp. 607–616, Jan. 2021.
[11] Y. Shen, H. Wang, A. Al-Durra, Z. Qin, and F. Blaabjerg, "A bidirectional resonant dc–dc converter suitable for wide voltage gain range," *IEEE Trans. Power Electron.*, vol. 33, no. 4, pp. 2957–2975, Apr. 2018.
[12] X. Lou, M. H. Ahmed, V. Li, and Q. Li, "Modeling and control of SingleStage 48 V sigma voltage regulator," *IEEE Trans. Ind. Electron.*, vol. 71, no. 7, pp. 7638–7649, Jul. 2024.
[13] Y. Cao, M. Ngo, N. Yan, D. Dong, R. Burgos, and A. Ismail, "Design and implementation of an 18-kW 500-kHz 98.8% efficiency high density battery charger with partial power processing," *IEEE J. Emerg. Sel. Topics Power Electron.*, vol. 10, no. 6, pp. 7963–7975, Dec. 2022.
[14] Z. Hou, D. Jiao, and J. -S. Lai, "An ultrawide range pulse width modulated LLC converter with voltage multiplier rectifiers," *Trans. Power Electron.,*vol. 40, no. 4, pp. 6216–6229, Apr. 2025.
[15] J. -W. Kim and P. Barbosa, "PWM-controlled series resonant converter for universal electric vehicle charger," *IEEE Trans. Power Electron.*, vol. 36, no. 12, pp. 13578–13588, Dec. 2021.
[16] H. Wang and Z. Li, "A PWM LLC type resonant converter adapted to wide output range in PEV charging applications," *IEEE Trans. Power Electron.*, vol. 33, no. 5, pp. 3791–3801, May 2018.
[17] Q. Zhao, W. Liu, Y. Wang, D. Wang, and N. Wu, "A novel multiresonant dc–dc converter with wide output-voltage range," *IEEE Trans. Power Electron.*, vol. 35, no. 6, pp. 5625–5638, Jun. 2020.
[18] X. Zhang, J. Jing, Y. Guan, M. Dai, Y. Wang, and D. Xu, "High-efficiency high-order CL-LLC dc/dc converter with wide input voltage range," *IEEE Trans. Power Electron.*, vol. 36, no. 9, pp. 10383–10394, Sep. 2021.
[19] P. Jin, J. Zhang, Y. Lu, Y. Guo, G. Lei, and J. Zhu, "Variable frequency isolated bidirectional CLLC resonant converter with voltage controlled variable capacitors," *IEEE Trans. Ind. Electron.*, vol. 70, no. 9, pp. 8907–8917, Sep. 2023.
[20] Y. Zuo, X. Pan, and C. Wang, "A reconfigurable bidirectional isolated LLC resonant converter for ultra-wide voltage-gain range applications," *IEEE Trans. Ind. Electron.*, vol. 69, no. 6, pp. 5713–5723, Jun. 2022.
[21] W. Sun, Y. Xing, H. Wu, and J. Ding, "Modified high-efficiency LLC converters with two split resonant branches for wide input-voltage range applications," *IEEE Trans. Power Electron.*, vol. 33, no. 9, pp. 7867–7879, Sep. 2018.
[22] Q. Zhao, J. Zhang, Y. Gao, D. Wang, and Q. Yang, "Hybrid variable frequency LLC resonant converter with wide output voltage range," *IEEE Trans. Power Electron.*, vol. 38, no. 9, pp. 11038–11049, Sep. 2023.
[23] Q. Zhao, J. Zhang, C. Fu, Y. Chen, and Q. Yang, "A structure-reconfigurable LLC resonant converter with wide gain range," *IEEE J. Emerg. Sel. Topics Power Electron.*, vol. 11, no. 4, pp. 4057–4067, Aug. 2023.
[24] G. Fan, X. Wu, T. Liu, and Y. Xu, "High-efficiency high-density MHz cellular DC/DC converter for on-board charger," *IEEE Trans. Power Electron.*, vol. 37, no. 12, pp. 15666–15677, Dec. 2022.
[25] Y. Xu, X. Dai, Z. Zhang, Z. Kang, and T. Jin, "A novel phase-shift pulse width modulation method for light-load bidirectional CLLC resonant converter," *IEEE Trans. Power Electron.*,vol. 38, no. 3, pp. 3257–3267, Mar. 2023.
[26] W. L. Malan, D. M. Vilathgamuwa, and G. R. Walker, "Modeling and control of a resonant dual active bridge with a tuned CLLC network," *IEEE Trans. Power Electron.*, vol. 31, no. 10, pp. 7297–7310, Oct. 2016.
[27] B.-K. Lee, J.-P. Kim, S.-G. Kim, and J.-Y. Lee, "An isolated/bidirectional PWM resonant converter for V2G(H) EV on-board charger," *IEEE Trans. Veh. Technol.*, vol. 66, no. 9, pp. 7741–7750, Sep. 2017.
[28] H. Wang, M. Shang, and D. Shu, "Design considerations of efficiency enhanced LLC PEV charger using reconfigurable transformer," *IEEE Trans. Veh. Technol.*, vol. 68, no. 9, pp. 8642–8651, Sep. 2019.
[29] C. Li, H. Wang, and M. Shang, "A five-switch bridge based reconfigurable LLC converter for deeply depleted PEV charging applications," *IEEE Trans. Power Electron.*, vol. 34, no. 5, pp. 4031–4035, May 2019.
[30] Z. Hou, D. Jiao, and J. -S. Lai, "A 500 kHz wide output LLC-T resonant converter with narrow frequency range, reduced circulating energy, and low voltage stress," *IEEE Trans. Power Electron.*, vol. 40, no. 8, pp. 11749–11762, Aug. 2025.

Qinglin Zhao received the B.S. degree in industrial automation from the Northeast Heavy Machinery College (which was renamed Yanshan University in 1997), Qiqihar, China, in 1992, and the M.S. and Ph.D. degrees in power electronics and power drives from Yanshan University, Qinhuangdao, China, in 2003 and 2007, respectively.

He is currently a Professor with the School of Electrical Engineering, Yanshan University. His research interests include high frequency and high efficiency power converters, and control of grid-connected inverters.

Zhouzhou Wu received the B.S. degree in electrical engineering and automation from Henan Polytechnic University, Jiaozuo, China, in 2023. He is currently working toward the M.S. degree in electrical engineering with Yanshan University, Qinhuangdao, China.

His main research interest includes high-frequency switching mode converter.

Shixiang Gao received the B.S. degree in electrical engineering and automation from the Henan University of Urban Construction, Pingdingshan, China, in 2020, and the M.S. degree in electrical engineering from Yanshan University, Qinhuangdao, China, in 2025.

His main research interests include bidirectional dc–dc resonant converter and server power supply system.

Jing Yuan received the B.S. degree in electrical engineering and automation from Shanxi Agricultural University, Jinzhong, China, in 2011, and the M.S. degree in electrical engineering from Yanshan University, Qinhuangdao, China, in 2014.

She is currently a Lab Technician with the School of Electrical Engineering, Yanshan University. Her research interests include control of grid-connected inverters and dc–dc converters.

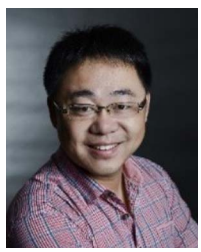

Deyu Wang (Member, IEEE) received the M.S. and Ph.D. degrees from the School of Electrical Engineering, Yanshan University, Qinhuangdao, China, in 2005 and 2009, respectively.

Since 2015, he has been an Associate Professor with the School of Electrical Engineering, Yanshan University. His main research interests include soft-switching dc–dc converters and wireless power transfer technology.

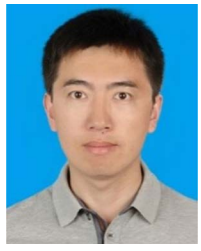

Hao Ding (Member, IEEE) received the B.S. and Ph.D. degrees in electrical engineering from Yanshan University, Qinhuangdao, China, in 2012 and 2017, respectively.

He is currently an Associate Professor with the Department of Electrical Engineering, Yanshan University. His current research interests include nonlinear and intelligent control for power converters and motor drives, stability and power quality of power-electronics-dominated power systems, high-power converters such as current source converter and modular multilevel converter.